

PAPER • OPEN ACCESS

Melt-quenched and as-deposited structures of amorphous selenium: a density functional/ molecular dynamics comparison

To cite this article: J Kalikka *et al* 2021 *J. Phys.: Condens. Matter* **33** 445401

View the [article online](#) for updates and enhancements.



IOP | ebooks™

Bringing together innovative digital publishing with leading authors from the global scientific community.

Start exploring the collection—download the first chapter of every title for free.

Melt-quenched and as-deposited structures of amorphous selenium: a density functional/ molecular dynamics comparison

J Kalikka¹ , K Konstantinou¹ , J Akola^{1,2}  and R O Jones^{3,*} 

¹ Computational Physics Laboratory, Tampere University, FI-33014 Tampere, Finland

² Department of Physics, NTNU Norwegian University of Science and Technology, NO-7491 Trondheim, Norway

³ Peter-Grünberg-Institut (PGI-1) and JARA/HPC, Forschungszentrum Jülich, D-52425 Jülich, Germany

E-mail: r.jones@fz-juelich.de

Received 25 June 2021, revised 11 July 2021

Accepted for publication 4 August 2021

Published 20 August 2021



CrossMark

Abstract

Molecular dynamics simulations using a density functional description of energies and forces have been carried out for a model of an as-deposited (AD) surface of amorphous selenium. The deposition model assumed the annealing (at 400 K) of layers of randomly located single atoms, followed by compression to the density used in earlier melt-quenched (MQ) simulations of amorphous Se, and by further annealing. The AD and MQ structures are predominantly twofold coordinated and similar, for example in the pair distribution functions, with notable differences: the AD structures have more defects (atoms with one and three neighbours), and the ring distributions differ. These differences are also reflected in the electronic structures of the AD and MQ samples, where the increased presence of defects in the former influences the Bader charges and the edge states of the band gap. The dominance of rings found in a previous simulation of AD structures is not found.

Keywords: amorphous selenium structure, molecular dynamics, density functional theory

(Some figures may appear in colour only in the online journal)

1. Introduction

Amorphous selenium (*a*-Se) has had important technological applications for decades, most recently in the field of sensors [1]. In its amorphous and liquid forms, selenium is also one of the best studied disordered materials and the only element that forms a stable glass at ambient temperatures. The unusual physical properties of disordered Se at temperatures near 300 K and above have provided a challenge for structural studies, the main point of controversy being the number of chains

and rings present in a particular sample [2]. There are at least six allotropes of the element [3, 4] comprising both chains and rings. The most stable form (*a*-Se, trigonal) is composed of parallel helical chains, and three monoclinic forms comprise Se₈ rings with different packings [4].

The composition of Se vapour depends on temperature and pressure [4, p 154], and there are extensive data at equilibrium of vapours containing Se and Se₂ [5] and Se_{*n*} molecules with *n* between 2 and 8 atoms [6]. Ring and chain isomers in group 16 elements show only small variations in bond lengths, bond angles, and dihedral angles [7–9], the main differences being the pattern of the *signs* of the dihedral angles ('motif' [10, 11]). Tuinstra [10] enumerated all possible molecular conformations with single values of bond length, bond angle, and magnitude of the dihedral angle, and determined the constraints required for ring closure. The total number of

* Author to whom any correspondence should be addressed.



Original content from this work may be used under the terms of the [Creative Commons Attribution 4.0 licence](https://creativecommons.org/licenses/by/4.0/). Any further distribution of this work must maintain attribution to the author(s) and the title of the work, journal citation and DOI.

conformations for n atoms is 2^{n-3} , and chain structures are generally much more numerous than rings, although the latter generally have an additional bond and lower energies [7–9]. Interconversion between rings and chains is an essential component of ring-opening polymerization in liquid sulphur [12].

Polymorphism occurring during vapour deposition can lead to ‘hidden’ glassy states that cannot be formed by slow cooling of a liquid [13], and recent molecular dynamics (MD) simulations on SiO_2 [14] indicate that the substrate temperature is important for the existence of such structures, which can be induced in a -Se *in situ* by light [15] or during vapour deposition [16]. Differences between bulk and surface structures are increasingly important in amorphous materials [15], and the vibrational dynamics and surface structure of a -Se have been interpreted in terms of overcoordinated defects near the surface [17]. Structures and photo-induced effects in elemental chalcogens, with particular focus on Raman scattering, have been reviewed recently [2].

The first MD simulations of vapour deposition of a -Se films [18, 19] considered individual Se atoms incident randomly on a crystalline substrate and interacting via tight-binding Hamiltonians and a classical three-body force field (FF) [20], whose parameters were chosen to reproduce the structures of small Se clusters and other properties of selenium. This FF has been used in many studies over the past 20 years [21], including a study of deposition from a vapour containing Se_n rings, with $2 \leq n \leq 8$ [22]. The structures were compared with available experimental data and with the results of early MD simulations of a -Se [23, 24] with density functional (DF) [25] calculations of energies and forces. Particular attention was paid to defect configurations. An analytical bond-order potential has been developed for the ternary system Cd–Te–Se using experimental information and selected DF results [26]. It was tested in MD simulations of vapour deposition of Se, resulting in the known crystalline structure, and this approach presents an attractive alternative for future work.

Experimental and theoretical work on amorphous and liquid Se was summarized recently [27], with particular focus on melt-quenched (MQ) phases, where a liquid sample is cooled slowly to a specified temperature. The viscosity of selenium changes by 12 orders of magnitude between the melting point (494 K) and the glass temperature (~ 300 K), and the history of a sample has a pronounced effect on its properties. Furthermore, the tendency of a -Se to crystallize spontaneously between 343 K and 441 K limits the availability of experimental data in this temperature range. The results of MD simulations of liquid and glassy Se were published recently [27], where the forces and energies were calculated using both DF methods and a classical FF [20]. These simulations covered different time and length scales (DF: 600 atoms, 140 ps, 400–773 K, FF: 5488 atoms, up to 800 ns, 290–500 K), with even larger samples being used in subsequent ageing studies [21]. There is good overall agreement with measured structural and dynamic properties, although the approaches lead to differences in the distributions of rings and chains, and the FF simulations indicate that the DF calculations below 500 K may be too short to ensure equilibration.

We report here results of DF/MD simulations on a model of the disordered ‘as-deposited’ (AD) surface of Se, which is sometimes referred to as ‘vapour deposited’. We avoid a bias towards rings or chains by assuming a random generation of atomic positions. The results are compared with previous work on MQ samples of a -Se, and we pay particular attention to the electronic structures of the two systems. We also compare the present AD results with those of the FF deposition simulations mentioned above [18, 19, 22]. Earlier DF/MD simulations on polymorphism in AD and MQ samples include work on $\text{Ge}_2\text{Sb}_2\text{Te}_5$ [28], where tetrahedrally bonded Ge atoms and homopolar bonds (including Ge–Sb) are favoured in the AD sample, and on GaSb and GaSb_7 [29], where Sb segregation is evident in the AD sample of the latter.

2. Methods of calculation

2.1. Density functional calculations

The DF/MD simulations were performed with the same program and input parameters as in [27], where full details (pseudopotential, energy cutoff for the plane wave basis, time step, thermostat) are provided. The PBEsol approximation [30] to the exchange–correlation energy was used, and the measured density of Se at the melting point (3.99 g cm^{-3} , number density $0.03043 \text{ atoms \AA}^{-3}$) was used in the MQ simulations for all temperatures. The density of a -Se has been somewhat controversial [31], and a value of 4.25 g cm^{-3} ($0.03240 \text{ atoms \AA}^{-3}$) has also been suggested [32].

An additional focus of this study is the electronic structure, particularly the states near the semiconducting gap, which is underestimated by the PBEsol and other generalized gradient or local density approximations. MQ calculations [27], for example, led to band gaps in the range 0.6–0.4 eV between 400 K and 600 K, compared with optical gaps close to 2 eV [33–35]. Improved agreement with experiment is often found with ‘hybrid’ approximations, where a fraction of exact exchange is added to the generalized gradient form. Here we use the PBE0 form [36] and the CP2K program [37], which uses a Gaussian basis set and an auxiliary plane-wave basis. The Se atoms were represented by a double- ζ (DZVP) Gaussian basis optimized for molecular structures, a kinetic energy cutoff of the plane wave basis of 400 Ry, and the Goedecker–Teter–Hutter pseudopotential [38]. The lowest energy MQ and AD structures were re-optimized for the PBE0 approximation using the Broyden–Fletcher–Goldfarb–Shanno method [39], and the electronic structure and charge distributions were determined for the final structures. The Bader ionic charges were computed from the total electronic density as described in [40].

2.2. Preparation of AD structure (DF/MD simulations)

The procedure used to generate the AD structure is shown in figure 1. The simulation cell was taken to have variable extent in the z -direction and square in the xy -plane with side (26.4567 \AA) such that a cube of this size would have the above experimental density. The structure was generated by first depositing a random substrate layer of 30 atoms in a thin

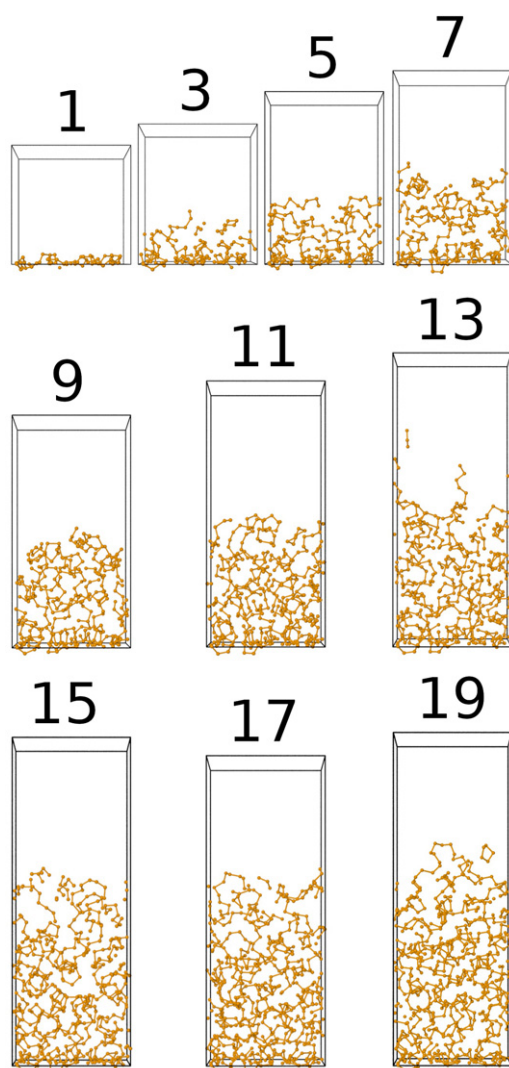


Figure 1. Visualization of layer-by-layer deposition at 400 K, shown for the odd-numbered layers. The final structure (19) is shown prior to compression. See text for more information.

(z -coordinate range was 0.5 \AA) square slab with 3.5 \AA minimum distance between atoms. The coordinates of the substrate atoms were then fixed throughout the deposition simulations. A succession of 19 sparse layers of 30 atoms each were generated and allowed to relax at 400 K on top of the existing structure, using the same minimum interatomic separation (3.5 \AA) until layer 16, when convergence difficulties in the orbital expansion led to an increase to 4.5 \AA . Each sparse layer was allowed to relax for 10 ps on top of the existing structure before the next layer was deposited, and the temperature was kept at 400 K throughout. The simulation cell was large enough in the z -direction that the interaction of each new layer with the bottom of the substrate layer was negligible.

The structure at this point contained a total of 20 layers (19 sparse layers and the fixed substrate layer) and was approximately twice as high as wide, with density approximately half of the experimental value. The structure was then compressed first by decreasing the z -dimension of the box so that the top atoms of the 19th layer were close to the bottom atoms of the

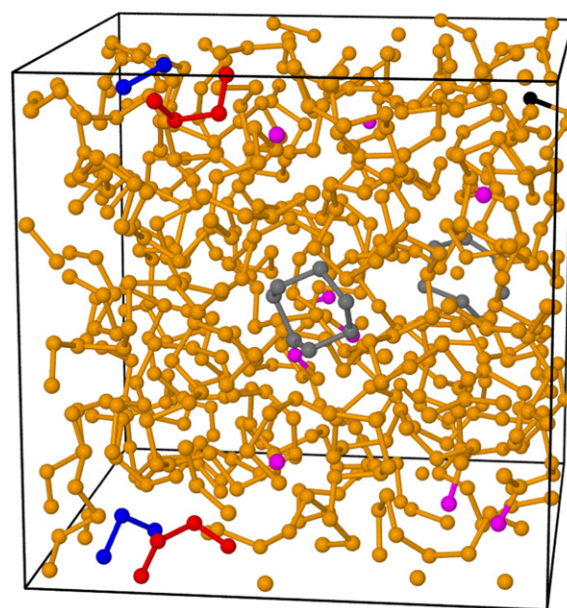


Figure 2. Final AD structure. Rings are shown with 5 (blue), 7 (green, grey), and 8 (red) atoms. Magenta atoms are singly coordinated (end of chain) and black denotes threefold coordinated (branch) atoms.

substrate, and then reducing the size by 0.1 \AA every ps, while allowing the structure to relax. The substrate atoms were no longer fixed and could relax as part of the structure. After 160 ps, the lateral size was adjusted from 26.4567 \AA to 27.0167 \AA over 6 ps to yield a cubic structure with density 3.99 g cm^{-3} ($0.03043 \text{ atoms \AA}^{-3}$) to allow a direct comparison with the MQ structures. The total length of the compression simulations was 253 ps, and data collection was carried out over 20 ps under conditions of constant particle number N , volume V , and temperature T at 400 K. The choice of this temperature represents a compromise between 300 K, where atomic motion is extremely sluggish, and the melting point (494 K).

3. Results

3.1. Structural properties

The structure at the end of data collection is shown in figure 2. Most of the atoms are in chains, but rings of five, seven, and eight atoms are evident. Singly coordinated atoms at chain ends and threefold coordinated atoms at branching points are also shown.

3.1.1. Pair distribution function, coordination numbers. The pair distribution function (PDF) gives the probability of finding pairs of atoms separated by a distance r . It is particularly useful in discussing short-range order in amorphous materials and was used in analyzing the FF simulations of vapour deposition mentioned above [18, 19, 22]. The pair distribution function (PDF) for the final AD structure (figure 3) has a pronounced minimum at 2.8 \AA , which is used to define the neighbours and the coordination number. Also shown are the

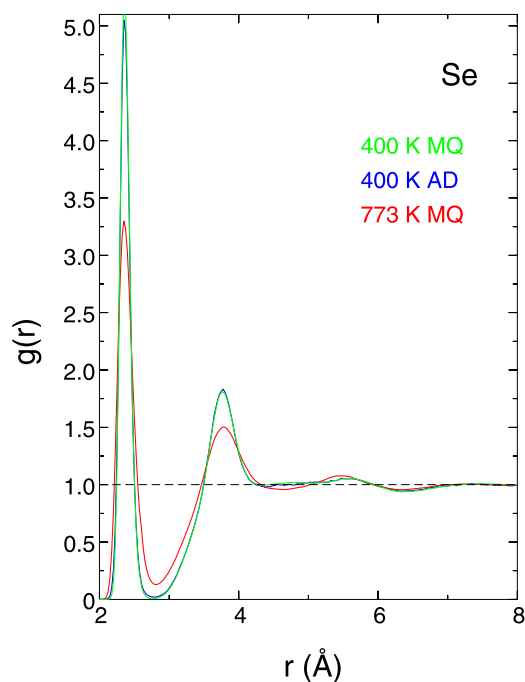


Figure 3. Pair distribution functions $g(r)$ for Se atoms in MQ samples at 400 K (green) and 773 K (red), and AD sample at 400 K (blue).

Table 1. Percentage of atoms with single (Se 1), twofold (Se 2), threefold (Se 3) and fourfold (Se 4) coordination in AD (left column) and MQ samples (remaining columns) at given temperatures.

	400 K AD	400 K	450 K	500 K	600 K	773 K
Se 1	1.02	0.02	0.05	0.10	0.26	2.17
Se 2	98.5	99.9	99.8	99.6	99.2	95.8
Se 3	0.46	0.10	0.17	0.29	0.57	2.02
Se 4	—	—	—	—	—	0.01

PDF for the MQ samples at 400 K and 773 K, and the AD and MQ functions at 400 K are clearly very similar. Twofold coordination of atoms of group 16 elements is very common [27], and this is true in all samples of *a*-Se considered here. In table 1 we show the percentage of atoms with coordination numbers between 1 and 4 in AD and MQ samples.

Most atoms have a coordination number of 2. Rings and chains are obvious candidates, and the main features of the MQ structures at 600 K and below were long chains [27]. However, the use of periodic boundary conditions in a cell with 600 atoms can make it difficult to distinguish between rings and chains near a cell boundary that can form closed loops under periodic constraints. If we limit consideration of rings to those with less than 30 atoms, up to 15% of the atoms in MQ structures and up to 25% of atoms in the AD structure are in rings.

3.1.2. Chains. On the basis of x-ray diffraction measurements on sulphur ring molecules and the sulphur helix, Steudel and co-workers [11, 41] found that the longest bonds are always adjacent to short bonds, with the bond length (d_2) being

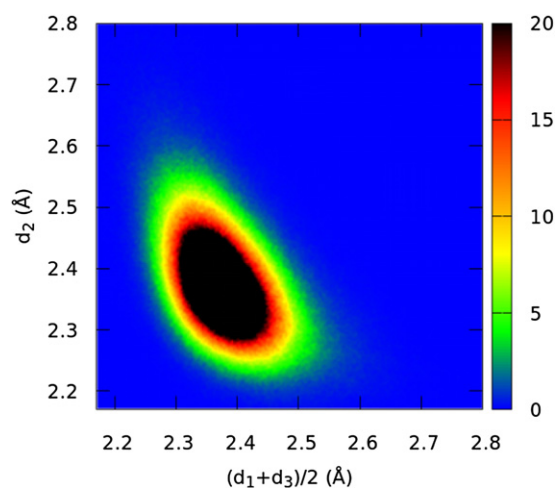


Figure 4. Colour map of bond lengths (d_2) of twofold-coordinated atoms against the average lengths of bonds to neighbouring atoms (d_1 and d_3) for AD *a*-Se. The origins of the axes correspond to the interatomic separation in Se_2 (2.17 Å).

approximately inversely related to the mean of the two neighbouring bonds (d_1 and d_3). Analyses of calculated bond lengths in S_n ring molecules ($n = 2-13$) [42] and S_n^- ions [43] found the same inverse relationship. Figure 4 shows colour maps of these two quantities for the AD simulations for all four-atom segments in rings and chains, where the central atoms are each twofold coordinated. The results show a slight shift to shorter side bonds in the tail, as also found in MQ simulations at 500 K [27].

The second empirical relation that was supported by calculations on S_n and S_n^- ring molecules is that d_2 is shortest for dihedral angles γ near 90° . For the same sequences of four atoms, we show the relationship between these quantities for the AD sample in figure 5. Dihedral angles near $\pm 90^\circ$ are preferred, and there are very few structures with γ near 0° , which occur in some Se_n isomers, or 180° , as found in the planar zigzag structure of the Se_∞ helix [44]. Structures with positive and negative dihedral angles are very similar, with a slight preference for positive dihedral angles. These results are again very similar to those in MQ samples at 500 K [27].

Structures with coordination numbers other than 2 are less common, but significant, as shown in table 1 and discussed for *a*-Se and related chalcogenide materials in [45]. Early DF/MD simulations indicated that single threefold coordinated atoms were the most common defect [23, 24]. Extended x-ray absorption fine structure measurements [15] showed that the coordination number increased to 2.2 after irradiation, indicating the formation of transient threefold coordination sites with a concentration of about 20%. The fractions found in the AD and MQ simulations are much lower than those found in a reverse Monte Carlo analysis of neutron diffraction measurements on liquid Se at 523 K and 623 K, where around 30% of the atoms were threefold- and around 5% fourfold-coordinated [46].

Bond angle distributions (for two- and threefold-coordinated atoms) are shown in figure 6. Also shown are the corresponding results for the MQ sample at 400 K, where there are fewer threefold-coordinated atoms. Apart from the

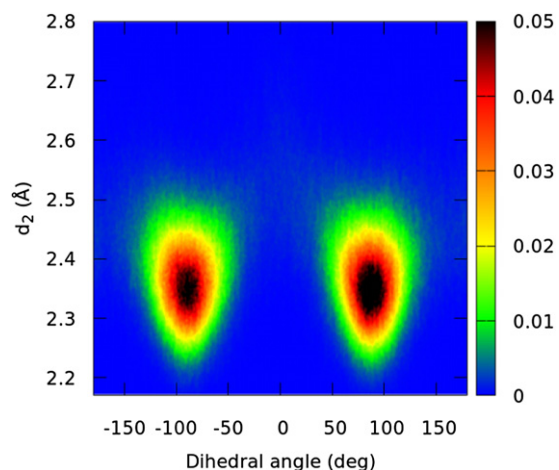


Figure 5. Colour map of bond lengths d_2 of twofold-coordinated atoms against dihedral angle γ for AD a -Se. The origin of the d_2 -axis corresponds to the interatomic separation in Se_2 (2.17 Å).

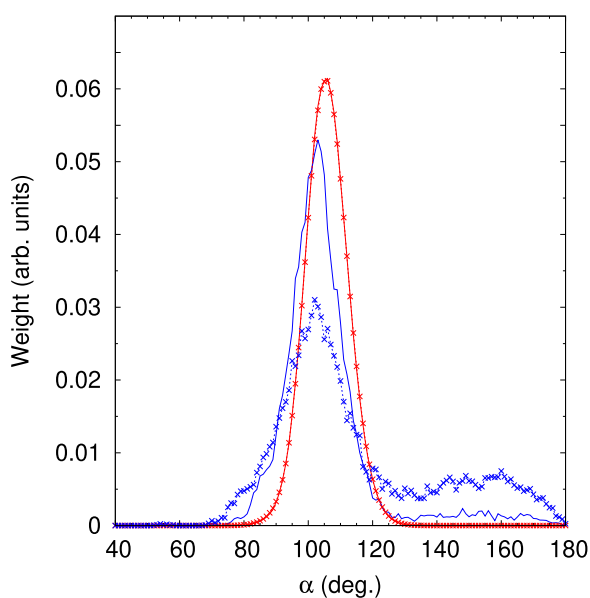


Figure 6. Distribution of bond angles α in AD a -Se for twofold- (red) and threefold-coordinated (blue) atoms. Crosses show the corresponding distributions for the MQ sample at 400 K [27].

prominent peaks ~ 100 – 110° , the distributions show few features, but the three-coordinated peak shows some weight at bond angles out to 180° , as in the MQ structures. The early DF/MD results [23, 24] are similar and also show enhanced weight for threefold-coordinated structures with $\alpha \sim 160^\circ$.

3.1.3. Rings. There have been many studies of rings in disordered chalcogens, as discussed in [27]. The ring distributions were determined here by enumerating all unique closed loops of bonded atoms, as described previously. The ring distributions in the AD samples show two dominant ranges, with 5, 6 and 8 members and 34, 36, and 38 members, and the distributions of rings containing 30 and fewer atoms are shown in figure 7 for a bond cutoff of 2.8 Å. Shorter cutoffs reduce the

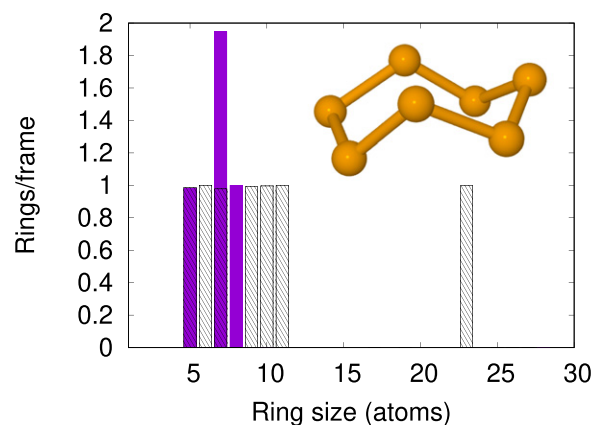


Figure 7. Average number of Se_n rings ($n \leq 30$) during simulations of AD a -Se (purple), as well as a Se_7 ring. The bond cutoff is 2.8 Å. Also shown (hatched) are the corresponding results for the MQ sample at 400 K [27].

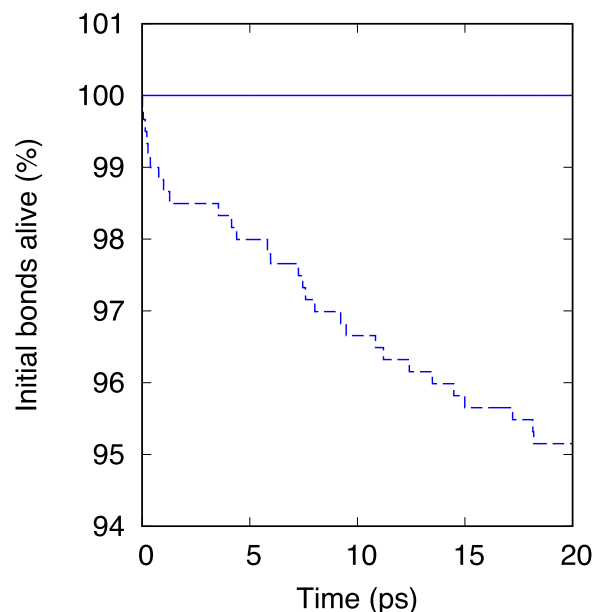


Figure 8. Time dependence of number of active bonds in AD a -Se simulation at 400 K during data collection (20 ps). Dashed curve: bonds break at 2.8 Å, full curve: bonds initially shorter than 2.4 Å, break at 3.8 Å.

number of rings, but the overall picture is unchanged. Seven-membered rings are the most common in the AD sample, where the average number of rings in the trajectory is 6.90 rings/frame. The Se_7 isomer in figure 7 is an example of a ring structure with a dihedral angle close to 0° .

The MQ structures showed wider distributions of ring sizes (figure 7) and an unexpected absence of Se_8 rings below 500 K [27]. The average number of rings per frame in the MQ structures was 7.64 for 400 K, 7.38 for 450 K, 7.11 for 500 K, 6.80 for 600 K, and 4.98 for 773 K.

3.1.4. Bond lifetimes. Bonds form and break at rates that depend on the temperature, and figure 8 shows the probability at 400 K that a bond shorter than 2.8 Å and present at time

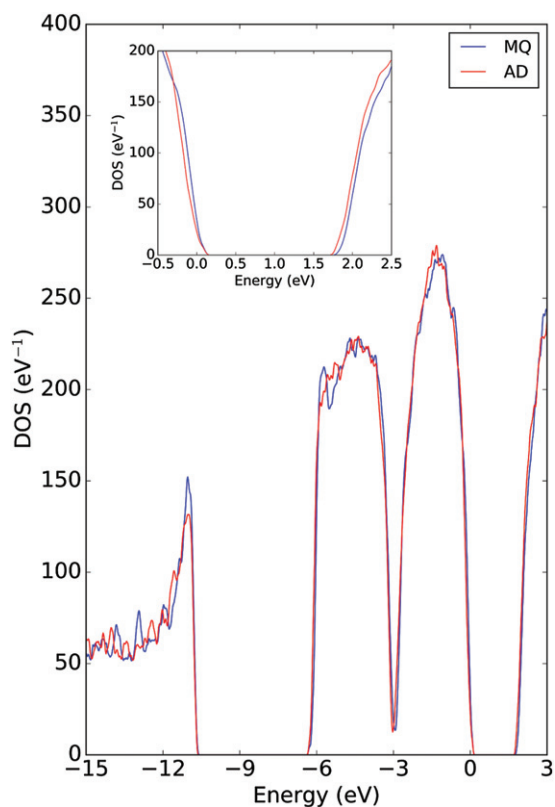


Figure 9. Comparison of electronic densities of states for MQ (blue) and AD (red) structures of *a*-Se. The inset shows the densities of states in the immediate neighbourhood of the gap.

$t = 0$ is also present at time t during the data collection phase (20 ps). The fixed bond cutoff may confuse ‘bond-breaking’ with bond stretching during vibration, and figure 8 also shows the variation with time of the number of bonds (shorter than 2.4 Å, but including those formed in the first 50 time steps) that are assumed to have ‘broken’ when they are longer than 3.8 Å. In the AD sample (400 K) and the MQ sample at 500 K, all bonds so defined exist throughout the simulation.

3.1.5. Cavities. Cavities were analyzed using the pyMolDYN program [47] with the cutoff distance r_c equal to 2.6 Å. The volume fraction of surface based cavities in the optimized AD sample of *a*-Se (48.5%) is very similar to the MQ structure values (48%–50%) and reflects the large interchain volume.

3.2. Electronic structure

The differences between the electronic densities of states for the MQ and AD samples (figure 9) are small, and the calculated gaps between the conduction and valence bands are 1.92 eV (MQ) and 1.87 eV (AD). The average values found for a series of snapshots taken during the PBEsol simulations were much smaller at the same temperature, being 0.59 eV (MQ) and 0.56 eV (AD). The measured gaps in an *a*-Se film prepared by plasma-enhanced chemical vapour deposition (1.94 eV) [34, 35] and in an *a*-Se powder (1.99 ± 0.02 eV) [33] are much larger. While a comparison between calculated and measured gaps must be treated with caution, the gaps for deposited samples are lower than the gaps in ‘bulk’ samples in experiment and in calculations using both functionals.

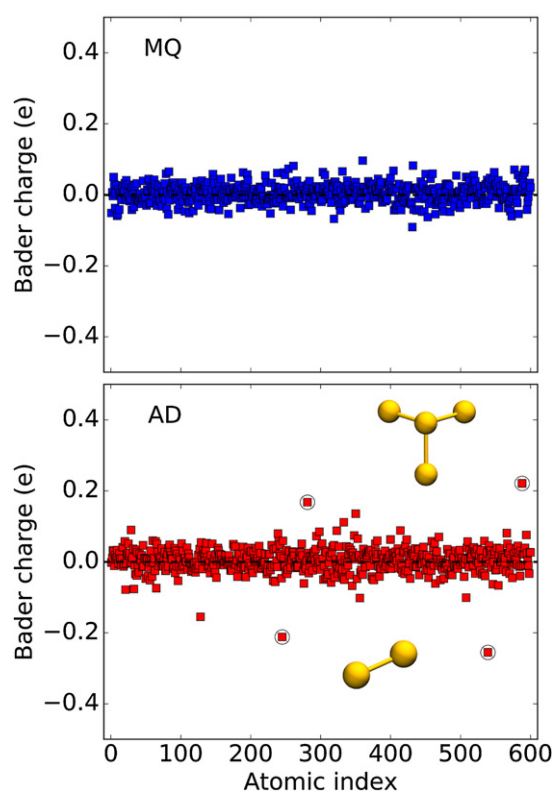


Figure 10. Comparison of Bader charges for MQ (blue) and AD (red) atoms at 400 K. The atoms corresponding to the defect structures are circled.

Bader [48] developed a scheme for dividing molecules into atomic regions based on the electronic charge density and surfaces where the density is a minimum. Bader charges for the atoms (figure 10) indicate that the number of one- and three-coordinated Se atoms in the AD sample is larger than in the MQ sample. The defect pair (figure 11, circled in figure 10) comprises a threefold coordinated atom with a positive Bader charge and a singly coordinated atom with a negative Bader charge and participates in the localization of the highest-occupied molecular orbital (HOMO) (figure 11).

4. Discussion

Results of DF/MD simulations (600 atoms) of a model of an ‘AD’ *a*-Se film have been compared with previous results for ‘MQ’ samples [27]. Deposition involved the random addition of Se atoms in a succession of 19 layers of 30 atoms each on a fixed Se monolayer, allowing annealing of each layer at 400 K for 10 ps. The resulting 20-layer structure was subjected to a slow compression and annealing at 400 K (0.1 \AA ps^{-1} , total simulation time 253 ps) until the density was equal to that chosen for the MQ samples. Direct comparison of the results is then possible.

The AD structure shows striking similarities to the MQ results below the melting point, which is consistent with the almost identical Raman spectra found in MQ samples of *a*-Se and in thin films of Se deposited at 383 K and annealed at lower temperatures [49]. The calculated structures are dominated by

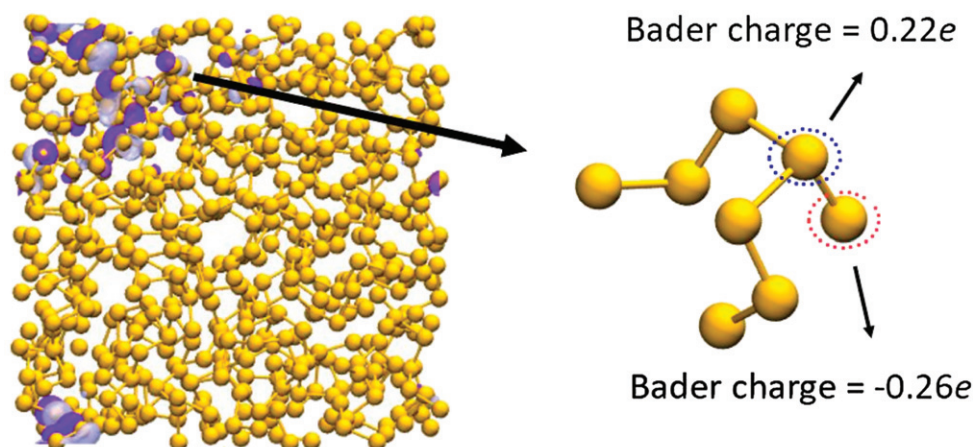


Figure 11. Se atoms are yellow, and the bond cutoff is 2.8 Å. The purple and blue isosurfaces (0.015 and -0.015 , respectively) illustrate the amplitude of the HOMO for the defect structure shown on the right.

twofold coordinated atoms, more in chains than in rings, a limited amount of branching at threefold coordinated sites, and some singly coordinated atoms at chain ends. Defect structures are more common in the AD sample than in all MQ samples. Pronounced similarities between MQ and a model AD structure obtained using a three-body classical FF [20] were also found for a model where deposition of single Se atoms was assumed [18, 19]. By contrast, an AD structure containing only rings was found in MD calculations [22] using the same FF if the vapour is assumed to contain rings of between 2 and 8 atoms according to their expected distribution in a vapour at 800 K. The same MD technique applied to MQ selenium led to chainlike structures [22].

We have noted that the composition of Se vapour depends dramatically on its thermodynamic state [4]. At equilibrium, the mole fraction of Se_n molecules [6] (figure 2) is completely different at 700 K (Se_6 dominates) and 1400 K (Se_2 dominates), and the vapour composition also depends very strongly on the method of production. Not only are the relative abundances of Se_n molecules quite different in vapours produced by laser irradiation at high temperature and pressure and by conventional (thermal) vaporization, but the relative abundances of neutral and ionic clusters differ profoundly [50]. Mass spectroscopy of charged species is a standard method for identifying atomic clusters in a vapour, and caution is needed when transferring information about charged clusters to the neutral distributions.

In addition to thermal and laser vaporization, Se vapour can be produced by field ionization and condensation [51, 52], plasma-enhanced chemical vapour deposition [34, 35], and pulsed laser deposition [17]. The resulting vapours can be far from thermodynamic equilibrium, and the most stable cluster isomers (usually rings in group 16 elements [7–9]) may not be the most prevalent. Under certain experimental conditions, for example, chain structures in sulphur cluster anions can be favored over ring structures with lower energies [43]. We have seen above that the number of chain structures can be much larger than the number of rings, for which ring-closing constraints on the pattern of dihedral angles must be satisfied [10].

Open structures with $\alpha \sim 120^\circ$ are more stable than triangular structures ($\alpha \sim 60^\circ$) in the trimers ozone O_3 [53], S_3 [8], and Se_3 [7].

The deposition procedure chosen here avoids assumptions concerning the cluster isomers present in the vapour, and the DF calculations of energies and forces describe both bond formation and breaking reliably in selenium. The absence of bias in favour of rings is a likely reason for the differences from the AD structure found in [22]. We caution, however, that our previous studies of MQ *a*-Se using DF/MD and classical FF simulations [27] emphasized the difficulty of equilibrating *any* calculation of disordered Se samples at temperatures significantly below the melting point (494 K).





Acknowledgments

We thank H R Schober for helpful discussions and acknowledge gratefully the computer time provided by the JARA-HPC Vergabegremium on the JARA-HPC partitions of the supercomputers JUQUEEN and JURECA (Forschungszentrum Jülich) and at the CSC-IT Centre for Science (Espoo, Finland). We thank the Academy of Finland for financial support through its NANOIONICS program (Project 322832).

Data availability statement

The data that support the findings of this study are available upon reasonable request from the authors.

ORCID iDs

J Kalikka  <https://orcid.org/0000-0001-7539-0785>
 K Konstantinou  <https://orcid.org/0000-0003-1291-817X>
 J Akola  <https://orcid.org/0000-0001-9037-7095>
 R O Jones  <https://orcid.org/0000-0003-1167-4812>

References

- [1] Masuzawa T *et al* 2013 *Sensors* **13** 13744–78 and references therein

- [2] Yannopoulos S N 2020 *J. Mater. Sci., Mater. Electron.* **31** 7565–95
- [3] Donohue J 1974 *The Structures of the Elements* (New York: Wiley)
- [4] Steudel R and Strauss E-M 1984 Homocyclic selenium molecules and related cations *Advances in Inorganic Chemistry* vol 28 ed H Emeléus and A G Sharpe (New York: Academic) pp 135–66 and references therein <http://sciedirect.com/science/article/pii/S089888380860207X>
- [5] Budininkas P, Edwards R K and Wahlbeck P G 1968 *J. Chem. Phys.* **48** 2867–9
- [6] Rau H 1974 *J. Chem. Thermodyn.* **6** 525–35
- [7] Hohl D, Jones R O, Car R and Parrinello M 1987 *Chem. Phys. Lett.* **139** 540–5
- [8] Jones R O and Ballone P 2003 *J. Chem. Phys.* **118** 9257–65
- [9] Akola J and Jones R O 2012 *Phys. Rev. B* **85** 134103 and references therein
- [10] Tuinstra F 1967 *J. Chem. Phys.* **46** 2741–6
- [11] Steudel R 1984 Elemental sulfur and related homocyclic compounds and ions *Sulfur, its Significance for Chemistry, for the Geo-, Bio-, and Cosmology and Technology (Studies in Inorganic Chemistry)* vol 5 ed A Müller and B Krebs (Amsterdam: Elsevier) pp 3–37
- [12] Ballone P and Jones R O 2003 *J. Chem. Phys.* **119** 8704–15
- [13] Dawson K J, Kearns K L, Yu L, Steffen W and Ediger MD 2009 *Proc. Natl Acad. Sci.* **106** 15165–70
- [14] Wang Z, Du T, Anoop Krishnan N M, Smedskjaer M M and Bauchy M 2020 *J. Chem. Phys.* **152** 164504
- [15] Kolobov A V, Oyanagi H, Tanaka K and Tanaka K 1997 *Phys. Rev. B* **55** 726–34
- [16] Zhang A, Jin Y, Liu T, Stephens R B and Fakhraai Z 2020 *Proc. Natl Acad. Sci.* **117** 24076–81
- [17] Scopigno T, Steurer W, Yannopoulos S N, Chrissanthopoulos A, Krisch M, Ruocco G and Wagner T 2011 *Nat. Commun.* **2** 195
- [18] Hegedüs J, Kohary K and Kugler S 2004 *J. Non-Cryst. Solids* **338–340** 283–6
- [19] Hegedüs J and Kugler S 2005 *J. Phys.: Condens. Matter* **17** 6459–68
- [20] Oligschleger C, Jones R O, Reimann S M and Schober H R 1996 *Phys. Rev. B* **53** 6165–73 Parameter a in table 1 should be 9281.2, $\alpha = -7.9284$
- [21] Schober H R 2021 *Phys. Rev. B* **103** 094202
- [22] Goldan A H, Li C, Pennycook S J, Schneider J, Blom A and Zhao W 2016 *J. Appl. Phys.* **120** 135101
- [23] Hohl D and Jones R O 1990 *J. Non-Cryst. Solids* **117–118** 922–5
- [24] Hohl D and Jones R O 1991 *Phys. Rev. B* **43** 3856–70
- [25] Jones R O 2015 *Rev. Mod. Phys.* **87** 897–923
- [26] Zhou X W, Foster M E, van Swol F B, Martin J E and Wong B M 2014 *J. Phys. Chem. C* **118** 20661–79
- [27] Kalikka J, Akola J, Jones R O and Schober H R 2020 *Phys. Rev. B* **102** 104202
- [28] Akola J, Larrucea J and Jones R O 2011 *Phys. Rev. B* **83** 094113
- [29] Kalikka J, Akola J and Jones R O 2013 *J. Phys.: Condens. Matter* **25** 115801
- [30] Perdew J P, Ruzsinszky A, Csonka G I, Vydrov O A, Scuseria G E, Constantin L A, Zhou X and Burke K 2008 *Phys. Rev. Lett.* **100** 136406
- [31] Jónvári P and Pusztai L 2001 *Phys. Rev. B* **64** 014205
- [32] Hansen F Y, Knudsen T S and Carneiro K 1975 *J. Chem. Phys.* **62** 1556–65
- [33] Bhatnagar A K, Reddy K V and Srivastava V 1985 *J. Phys. D: Appl. Phys.* **18** L149–53
- [34] Nagels P, Sleetckx E, Callaerts R and Tichy L 1995 *Solid State Commun.* **94** 49–52
- [35] Tichý L, Tichá H, Nagels P, Sleetckx E and Callaerts R 1996 *Mater. Lett.* **26** 279–83
- [36] Perdew J P, Ernzerhof M and Burke K 1996 *J. Chem. Phys.* **105** 9982–5
- [37] Kühne T D et al 2020 *J. Chem. Phys.* **152** 194103 and references therein
- [38] Goedecker S, Teter M and Hutter J 1996 *Phys. Rev. B* **54** 1703–10
- [39] Fletcher R 1970 *Comput. J.* **13** 317–22 and references therein
- [40] Henkelman G, Arnaldsson A and Jónsson H 2006 *Comput. Mater. Sci.* **36** 354–60
- [41] Steudel R and Eckert B 2003 Solid sulfur allotropes *Elemental Sulfur and Sulfur-Rich Compounds I* ed R Steudel (Berlin: Springer) pp 1–80 and references therein
- [42] Hohl D, Jones R O, Car R and Parrinello M 1988 *J. Chem. Phys.* **89** 6823–35
- [43] Hunsicker S, Jones R O and Ganteför G 1995 *J. Chem. Phys.* **102** 5917–36
- [44] Springborg M and Jones R O 1988 *J. Chem. Phys.* **88** 2652–8
- [45] Steudel R 1986 *J. Non-Cryst. Solids* **83** 63–79 and references therein
- [46] Maruyama K, Tamaki S, Takeda S and Inui M 1993 *J. Phys. Soc. Japan* **62** 4287–94
- [47] Heimbach I, Rhiem F, Beule F, Knodt D, Heinen J and Jones R O 2017 *J. Comput. Chem.* **38** 389–94
- [48] Bader R F W 1990 *Atoms in Molecules: A Quantum Theory* (Oxford: Oxford University Press)
- [49] Carroll P J and Lannin J S 1981 *Solid State Commun.* **40** 81–4
- [50] Ban V S and Knox B E 1969 *Int. J. Mass Spectrom. Ion Phys.* **3** 131–41
- [51] Saure H and Block J 1971 *Int. J. Mass Spectrom. Ion Phys.* **7** 145–55
- [52] Saure H and Block J 1971 *Int. J. Mass Spectrom. Ion Phys.* **7** 157–66
- [53] Jones R O 1985 *J. Chem. Phys.* **82** 325–32